





RESEARCH ARTICLE

10.1029/2023JG007450

Sea-Level Rise Impacts on Tidal Marshes and Estuarine Biogeochemical Processes

Xun Cai^{1,2} , Jian Shen¹ , Yinglong J. Zhang¹ , Qubin Qin^{1,3} , and Lewis Linker⁴

¹Virginia Institute of Marine Science, William & Mary, Gloucester Point, VA, USA, ²ORISE Research Participation Program at EPA, Chesapeake Bay Program Office, Annapolis, MD, USA, ³Now at Department of Coastal Studies, East Carolina University, Wanchese, NC, USA, ⁴U.S. Environmental Protection Agency Chesapeake Bay Program Office, Annapolis, MD, USA

Key Points:

- A coupled tidal marsh and eutrophication model is applied to study the impacts of sea-level rise (SLR) on estuarine biogeochemical processes
- The tidal marshes that keep up with SLR are predicted to have more porewater-surface water exchange and dissolved material exports
- The York River Estuary is predicted to have lower bottom dissolved oxygen and more hypoxia events under SLR

Correspondence to:

X. Cai,
ncai@vims.edu;
xcai@chesapeakebay.net

Citation:

Cai, X., Shen, J., Zhang, Y. J., Qin, Q., & Linker, L. (2023). Sea-level rise impacts on tidal marshes and estuarine biogeochemical processes. *Journal of Geophysical Research: Biogeosciences*, 128, e2023JG007450. <https://doi.org/10.1029/2023JG007450>

Received 25 FEB 2023
 Accepted 14 AUG 2023

Author Contributions:

Conceptualization: Xun Cai, Jian Shen, Qubin Qin
Data curation: Xun Cai
Formal analysis: Xun Cai, Jian Shen, Qubin Qin
Funding acquisition: Yinglong J. Zhang, Lewis Linker
Investigation: Xun Cai, Jian Shen
Methodology: Xun Cai, Jian Shen, Yinglong J. Zhang
Project Administration: Yinglong J. Zhang, Lewis Linker
Resources: Lewis Linker
Software: Xun Cai, Yinglong J. Zhang
Supervision: Jian Shen, Yinglong J. Zhang
Validation: Xun Cai, Qubin Qin
Visualization: Xun Cai
Writing – original draft: Xun Cai

Abstract We used a numerical model to investigate the effects of sea-level rise (SLR) on the biogeochemical processes in the York River Estuary with extensive tidal marshes. The fully-coupled hydrodynamic-water quality-marsh model accounts for the spatial and temporal variations of physical-biogeochemical interactions between the tidal marshes and surrounding waters. This study focuses on an SLR scenario where the vertical accretion of tidal marshes keeps pace with the rising sea levels. Results show that SLR amplifies the tidal range and prolongs flooding duration, which results in enhanced porewater exchanges of materials between the tidal marshes and the surrounding waters. The increased availability of shallow-water habitats and enhanced light utilization in the shallow areas under SLR promote phytoplankton production (PP) in the shallow-water regions of the York River. Consequently, the organic carbon in the open water is fueled by the contributions from shallow waters and the enhanced export of organic carbon from the marshes. The change in the dissolved oxygen (DO) budget in the York River Estuary is attributed to changes in water column respiration, net metabolism of the benthic layer, reaeration, PP, and increased stratification under SLR. The net DO flux out of the York River increases at the York River mouth. Diel DO variation, especially in the marshes in the upper estuary, promotes phosphorus release from the sediment. The changes in dissolved nitrogen under SLR are relatively minimal.

Plain Language Summary As one of the consequences of climate change, sea-level rise (SLR) has a wide-ranging impact on the estuarine environment. SLR has a significant impact on tidal marshes, which are located at the interface between estuarine water and inner land. Despite the possibility of marsh retreat, many tidal marshes will keep up with the SLR through vertical accretion if sufficient sediment sources are available. SLR will result in deeper water and elevated tidal marshes in the estuary. The biogeochemical processes under this condition were predicted using a numerical modeling approach in this study. The tidal range is estimated to increase, encouraging more material exchange between marshes and estuarine water. More organic carbon is produced in this system, resulting in increased oxygen consumption. In this condition, there is a greater likelihood of low-DO events occurring during the diel cycle, which will further affect nutrient dynamics.

1. Introduction

Sea-level rise (SLR) is well known to affect both physical (e.g., tidal range, salinity, and estuarine circulation) and biogeochemical processes (e.g., phytoplankton production (PP), and nutrient dynamics) in estuaries. The response of the estuarine biogeochemical processes to SLR can be considered as a combination of changes in both the physical and biogeochemical processes. The impact of SLR on the tidal marshes can affect the estuarine circulation and water quality. With SLR, tidal marshes experience a geomorphological evolution along with ecological succession, dominated by the rise of the platform through vertical accretion or the drowning of mudflats from erosion (Boon, 2012; Craft et al., 2009). SLR also affects the ecological functions of tidal marshes, which in turn affects the oxygen and nutrient dynamics in estuaries (Axelrad et al., 1976; Bridgman et al., 2006; Chambers, 1992; Chmura et al., 2003; Jordan et al., 1983). For example, different responses of the tidal range to SLR are a major factor for the material exchange between marshes and open water. In previous studies, Cai et al. (2022) emphasized the role of marsh evolution that led to different responses of tidal range to the SLR in tidal wetlands. If the tidal marsh accretion can keep up with the SLR, the tidal range is projected to increase. The increased tidal range will further strengthen the exchanges between the marsh and the mainstem estuary. Increased flux of saltwater from the oceanside is another major consequence of rapid relative SLR in an estuary

© 2023. The Authors.

This is an open access article under the terms of the [Creative Commons Attribution License](https://creativecommons.org/licenses/by/4.0/), which permits use, distribution and reproduction in any medium, provided the original work is properly cited.

Writing – review & editing: Xun Cai, Jian Shen, Yinglong J. Zhang, Qubin Qin, Lewis Linker

(Bates et al., 2008; Boon, 2012; Hong et al., 2020). As a result, there is observable evolution from freshwater marsh to brackish marsh in the community structure in response to the enhanced saltwater intrusion (Neubauer & Craft, 2009; Sutter, 2014). The shifts in community structure may affect the ecological function of tidal marshes due to the distinct roles played by each marsh plant group. Another key factor in the persistence of tidal marshes under SLR conditions is the ability of landward migration (Molino et al., 2022).

Besides impacts on the tidal marshes, SLR also affects local nutrient dynamics directly. For example, increased salinity under the enhanced saltwater intrusion is favorable for the bottom release of phosphorus that is bound to iron (Fe) oxyhydroxides, which tends to have enhanced dissolution under higher salinity (Jordan et al., 2008). Salinization also tends to alter the microbial community composition or inhibit microbial activity, which inhibits nitrification and coupled nitrification-denitrification (Rysgaard et al., 1999; Santoro, 2010). Also, ammonium absorption in sediments is found to markedly decrease with increased salinities (Rysgaard et al., 1999). The above two processes lead to enhanced bottom ammonium flux. Furthermore, SLR is predicted to change the benthic-pelagic coupling and increase the water column PP by changing the local bathymetry and light utilization in shallow shoals (Cai et al., 2021). Along with the potential changes in the nutrient exchange between the tidal marshes and the adjacent channel, as well as the sediment nutrient release, the local PP could be altered. In short, the feedback loop between SLR and marsh is complex and nonlinear in nature, resulting in large uncertainties in future predictions and thus warrants careful research using a variety of tools.

Considering the nonlinear responses of physical and biogeochemical processes to SLR, numerical modeling may be one of the best approaches to understanding the impacts of SLR on the aquatic system, as it can be built to account for various ecological functions. Many numerical studies have investigated the impacts of SLR on some estuarine biogeochemical processes (e.g., hypoxia), but few of them have included the tidal marshes explicitly in the model (Cai et al., 2021; Irby et al., 2018; St-Laurent et al., 2019; P. Wang et al., 2017). For a few models that did consider the contributions of marsh to nutrient burial and exports (e.g., Cerco & Tian, 2022), the process was often simplified, because the tidal marshes were not explicitly represented in the estuarine model grid and the tidal flooding and inundations under SLR were not simulated. In addition, the loss rates of the nutrients and DO for marshes under SLR were unknown and sometimes were assumed to be the same as the current situations. In this study, a high-resolution three-dimensional unstructured-grid (UG) hydrodynamic-water quality-marsh model is used to investigate the impacts of SLR on biogeochemical processes in the York River Estuary, a typical microtidal estuary in the lower Chesapeake Bay where extensive tidal marshes exist. The inclusion of a dynamic marsh module helps to investigate the responses of the tidal marshes to SLR and the consequent impacts on the estuarine biogeochemical processes with sufficient spatial and temporal variations. This paper is organized as follows: descriptions of the modeling tool, scenario, and analysis methods are presented in Section 2. Responses of the estuarine biogeochemical processes, including the tidal marsh, nutrients, PPs, and oxygen dynamics, are presented in Section 3. Section 4 presents the discussions on the physical drivers contributing to the responses of the estuarine biogeochemical processes, with specific analysis of the oxygen dynamics in different sections of the York River Estuary. Section 5 summarizes the entire study and proposes a conceptual model for the impact of SLR on the York River Estuary.

2. Methods

2.1. SCHISM-ICM-Marsh Model

We use a fully coupled hydrodynamic, water quality, and marsh model (SCHISM-ICM-Marsh) for this study (Cai et al., 2020, 2023a; Cerco & Cole, 1994; Zhang et al., 2016). SCHISM is Semi-implicit Cross-scale Hydroscience Integrated System Model and Integrated Compartment Model (ICM) is ICM multi-dimensional water quality model. SCHISM-ICM-Marsh solves the physical and biogeochemical processes simultaneously and accounts for the interactions between the marsh and the aquatic system. It is designed for simulations on seasonal and annual time scales. A distinctive advantage of SCHISM is its semi-implicit time-stepping scheme, implemented in a hybrid finite-element and finite-volume framework, to solve Navier-Stokes equations. All terms that place stringent stability constraints, including the vegetation drag terms are treated implicitly, so the model time step is not restricted by the Courant-Friedrichs-Lewy condition or the vegetation terms in this numerical scheme. This numerical scheme ensures high efficiency because not only high resolution is required to resolve the patchy marshes, but also the “nearly submerged” marsh leaves and the resultant strong shears would otherwise impose a severe stability constraint (Zhang et al., 2020). There are 21 water quality state variables in ICM, including DO, sulfide, three algal assemblages (diatoms, green algae, and cyanobacteria), three groups of carbon (dissolved, labile particulate,

and refractory particulate organic carbon), five groups of nitrogen (ammonium, nitrate, dissolved, labile particulate, and refractory particulate organic nitrogen), four groups of phosphorus (phosphate, dissolved, labile particulate, and refractory particulate organic phosphorus), and two groups of silica (particulate biogenic silica and total available silica) (Cai et al., 2020; Cerco & Cole, 1994). Three marsh assemblages, comprised of tidal freshwater marsh, brackish marsh, and salt marsh, are included in the coupled marsh model. Each marsh species consists of three components—leaf, stem, and root. SCHISM simulates the transport of the 21 water quality state variables, while the coupled ICM-Marsh simulates the local kinetic processes of the 21 state variables and the three marsh plants. In addition, benthic algae are included in the water quality model to account for their productivity and interactions with the carbon, oxygen, nitrogen, and phosphorus pools (Cerco & Seitzinger, 1997).

2.2. Study Area

The York River Estuary comprises the York River, Pamunkey River, and Mattaponi River, where the York River starts from the confluence of the Pamunkey River and Mattaponi Rivers at West Point. It is the fifth biggest tributary in the Chesapeake Bay. The length of the York River is about 50 km from West Point to Goodwin Island. In the Pamunkey and Mattaponi Rivers, the tidal portion extends about 90 and 70 km from the West Point, respectively (Brooks, 1983, <http://water.usgs.gov>). The average width of the York River is 3.8 km while the meandering Pamunkey River and Mattaponi Rivers are several hundreds of meters wide (Nichols et al., 1991). The York River downstream of West Point has an average water depth of 4.9 m, and the channel depth is up to 20 m at Gloucester Point (Cronin, 1971; Nichols et al., 1991). With the Pamunkey and Mattaponi Rivers and the tidal marshes included, the mean depth of the whole York River Estuary is shallower than the reported 4.9 m downstream of West Point. Therefore, a SLR of 1.5 m would increase the mean local depth by at least 30%, which may significantly alter many local processes.

In the York River Estuary, the annual high and low temperatures are ~ 35.7 and $\sim 0.9^\circ\text{C}$, respectively with a clear seasonal trend (Brooks, 1983). The average precipitation is about 95.9 cm. Waves are usually considered to be insignificant for this region (Friedrichs, 2009). The York River estuary is a micro-tidal estuary, whose mean tidal range increases from 0.7 m at the mouth to more than 1 m in upstream of the Pamunkey and Mattaponi Rivers (https://tidesandcurrents.noaa.gov/historic_tide_tables.html). The tidal range at the extensive tidal marshes is from about 0.75 m to about 1 m. The bottom salinity at the York River mouth can exceed 25 PSU, with a range of 0–20 PSU at the West Point dependent on the freshwater discharge (<https://www.chesapeakebay.net/what/data>). The upper portion of the Pamunkey and Mattaponi Rivers are mostly tidal fresh with a transition zone near the West Point (Shen & Haas, 2004). The mean freshwater discharge from the Pamunkey River and Mattaponi Rivers are 28.7 and 14.4 $\text{m}^3 \text{s}^{-1}$, respectively; and the York River Estuary has a mean residence time of 104 days (Shen & Haas, 2004).

The river discharge in the York River Estuary has been recognized as a main control that regulates the phytoplankton dynamics temporally and spatially by residence time, nutrient loading, light regime, and tidal mixing (Sin et al., 1999). Phytoplankton dynamics and productivity in the York River Estuary are mainly regulated by nutrient supply and light availability utilization (Sin et al., 2006). Limitations from dissolved inorganic nitrogen (DIN), phosphate, and light shift the governing role of regulation temporally and spatially (Sin et al., 1999, 2006). The agricultural land, urban areas, and forested lands dominate the nutrient loads to the York River Estuary with the total nitrogen loading on the order of $3.5 \times 10^6 \text{ kg yr}^{-1}$ and total phosphorus loading on the order of $3.4 \times 10^5 \text{ kg yr}^{-1}$ (Dauer et al., 2007; Sprague, 2000). Hypoxia (defined as DO concentration lower than 2 mg L^{-1}) or under-saturation of DO by 50% has often been observed in the York River in summer (Kuo & Neilson, 1987). In addition to the observed hypoxia in the channel, diel variation in DO is also observed in temperate unstratified shallow waters and habitats (Reay, 2009).

Excluding the embayed tidal marshes in the sub-tributaries, there are about 50.6 km^2 of extensive tidal marshes in the York River Estuary, which account for almost 97.27% of the total marsh coverage in the entire York River estuary (Mitchell et al., 2017). Although experiencing community shifts from freshwater species to brackish ones, the areal extent of marshes in the upper York River Estuary (Pamunkey and Mattaponi Rivers) was reported to have changed little ($<0.009\%$) over the past three decades (Mitchell et al., 2017; Sutter, 2014), so the marshes were believed to have sufficient vertical accretion with both sufficient marsh productions and allochthonous sediments to keep up with the SLR (Mitchell et al., 2017; Neubauer & Craft, 2009).

In this study, we selected the Sweet Hall Marsh (Figure 1c) to present spatial variations of changes in marsh productivity, as it is an active observation site where ongoing observations are being conducted. We also selected four sampling stations at the Sweet Hall Marsh for further analysis of temporal variation, including two stations in the marsh bed and adjacent tidal ditch, respectively (Figures 1c and 10) and two stations that exhibit bifur-

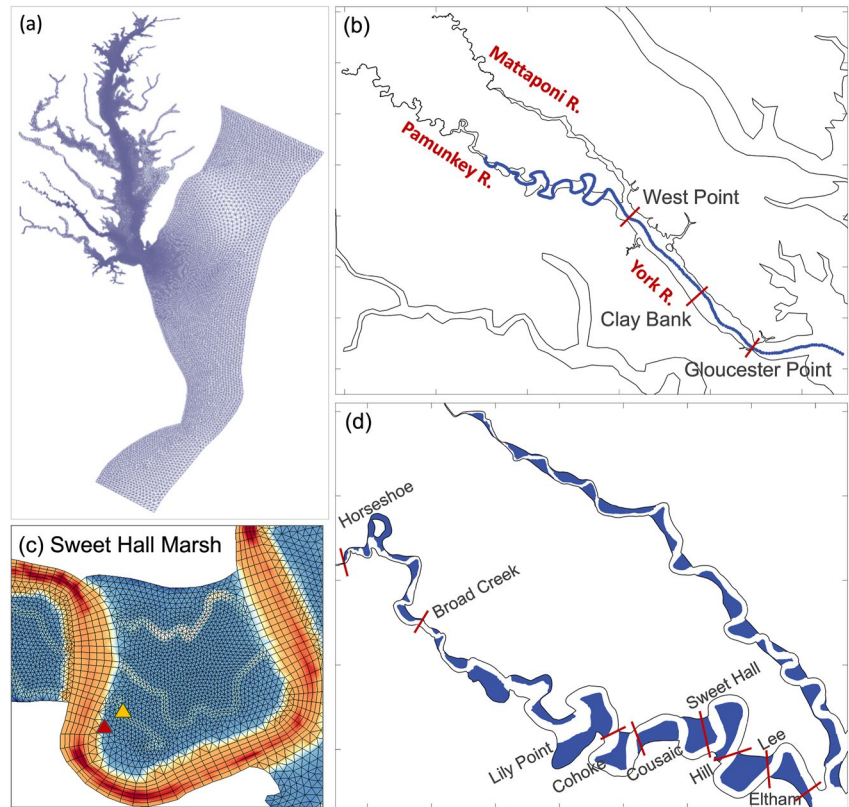


Figure 1. (a) Model domain with local refinement in the York River Estuary. (b) The York River Estuary with a blue line that denotes the along-channel transect used in this study. (c) Sweet Hall Marsh. Red and yellow triangles denote the sampling points of diel processes in the marsh bed and adjacent ditch, respectively for the analysis in Figure 10c. (d) Extensive and fringing marshes in the study area. The red lines in panels (b) and (d) denote the transects to calculate the material exchange in this study. Based on the USGS topography map, the blue polygons in (d) mark the marshes along the Pamunkey and Mattaponi Rivers.

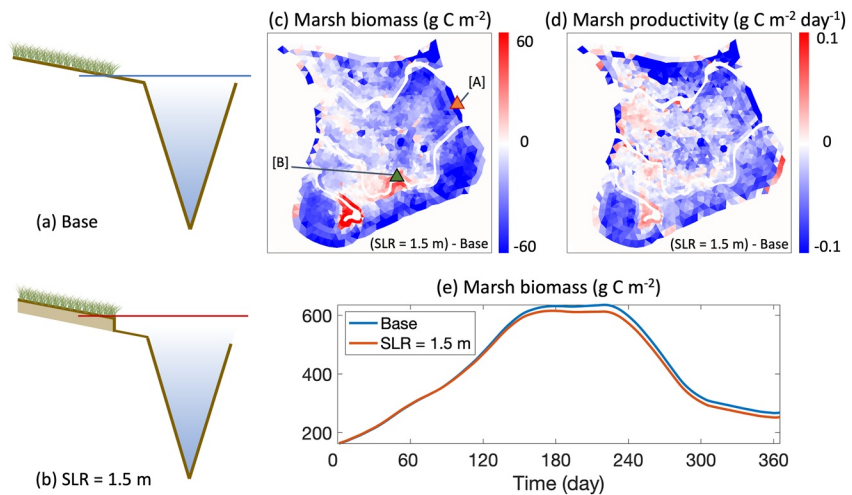


Figure 2. (a, b) Diagrams of the Base and sea-level rise (SLR) scenarios, where marsh keeps up with the rising sea-level of 1.5 m. (c, d) Absolute difference ((SLR = 1.5 m) – Base) of annual averages of marsh biomass and net marsh productivity in Sweet Hall Marsh. Orange and green triangles in (c) denote the sampling points for analysis in Figure 3. (e) Spatial averages of marsh biomass in the York River Estuary in Base and SLR = 1.5 m Scenario. The marsh area is denoted in Figure 1.

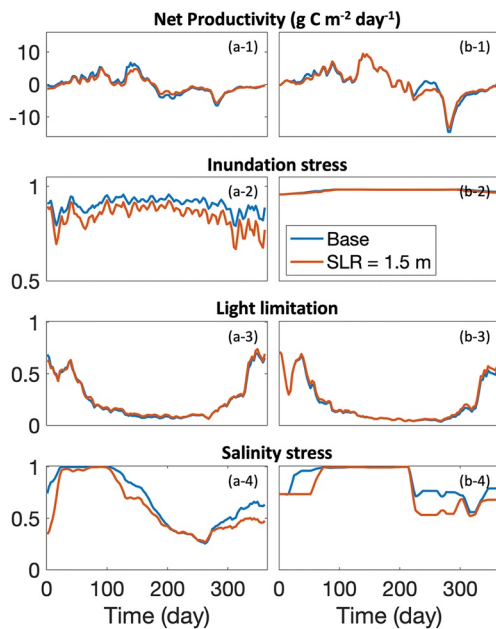


Figure 3. Response of marsh net productivity, inundation stress, light limitation, and salinity stress to sea-level rise in multiple sampling locations in the Sweet Hall Marsh. Sampling locations are denoted in Figure 2c. The marsh biomass and productivity decrease at location (a) and increase at location (b).

to the upstream, while the cross-channel resolution ranges from 200 m to less than 50 m to ensure that at least six rows of elements are used to accurately represent the channel. A hybrid vertical grid system LSC² (Localized Sigma Coordinates with Shaved Cells) with up to 52 vertical layers and one layer for the shallow wetlands is applied in this domain.

cate responses on marsh productivity under SLR based on preliminary model results (Figures 2c and 3). By conducting a comprehensive modeling analysis, there is the potential to establish meaningful connections between observations in this region for future purposes. We selected a continuous transect along the deep channel from the mouth of the York River to the upper stream of the Pamunkey River to compare significant water properties between scenarios (Figures 1b, 4, and 6). We used the entire area of the York River Estuary, including the three channels and all wetlands, to estimate the PP (Figure 5). Furthermore, we calculated material fluxes and DO budget analysis on 11 selected cross-channel transects from the York River mouth to the upper stream of the Pamunkey River (Figures 1b, 1d, 7, 8, and 9). Although the Mattaponi River was not explicitly depicted in certain figures due to its similarity to the Pamunkey River, it was consistently included in our analysis.

2.3. Model Implementation and Scenarios

Base Scenario simulation uses the current mean sea level as a reference datum for model simulations, and the model has been developed and calibrated by Cai et al. (2023a) for the years 2010–2014 with a single non-split time step of 150 s. The base simulation period for SLR scenarios is the year of 2010, which is regarded as an average flow year. The ocean boundary extends offshore to the shelf break to minimize the influence of open ocean conditions on the interior of the Bay and the York River Estuary. This grid contains 47,477 nodes and 73,433 elements, and the prevailing resolution in the extensive marshes in the York River Estuary (e.g., Sweet Hall Marsh) is about 50 m. In the rest part of the York River estuary, the along-channel resolution ranges from 300 to 100 m from the mouth

Interpolated elevations from two tidal gauges at Lewes, DE, and Beaufort, NC were used to force elevations at the ocean boundary. The boundary temperature is obtained from the hybrid coordinate ocean model (HYCOM, Chassignet et al., 2007) and the boundary salinity is from World Ocean Atlas monthly climatological data. Groundwater discharge was not explicitly simulated or included. The daily runoff and nutrient loads were generated from the Phase 6 Watershed Model of the Chesapeake Bay Assessment Tool (Shenk & Linker, 2013). We obtained the atmospheric forcing and heat fluxes from the North American Regional Reanalysis (Mesinger et al., 2006). The marsh extent was initialized using the USGS topography map (https://www.usgs.gov/core-science-systems/national-geospatial-program/us-topo-maps-america?qt-science_support_page_related_con=0#qt-science_support_page_related_con).

SLR scenarios of 1.5, 1.0, and 0.5 m were added to the sea surface height at the ocean boundary of the Base Scenario to the SLR scenario. The SLR scenario of 1.5 m was mainly used in this study to study the response of the biogeochemical processes, while the rest were used as sensitivity tests. The defined marsh wetlands also had an increase of 1.5, 1.0, and 0.5 m on the bottom elevation by assuming the vertical accretion of these marshes keep up with the SLR without changing the horizontal expansion (Figures 1d, 2a, and 2b; Cai et al., 2022). This idealized SLR-driven marsh evolution (keeping up with the SLR) avoids an explicit simulation of long-term marsh migration (which is beyond the seasonal and annual time scales simulated by the current model). We focused on the dynamic changes in the biogeochemical processes under this hypothetical scenario. The Base and SLR scenarios share identical

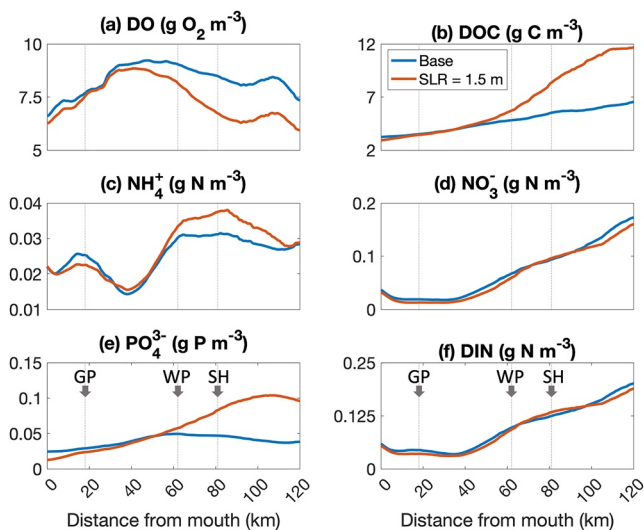


Figure 4. Comparisons of Base Scenario and sea-level rise scenario of 1.5 m of bottom dissolved oxygen and other surface water properties, including ammonia, nitrate, phosphate, and dissolved organic carbon, along the channel of Pamunkey and York Rivers. The along-channel transect is denoted in Figure 1b. Locations of Gloucester Point, West Point, and Sweet Hall are denoted in panel (e) along with gray dotted lines in all the panels.

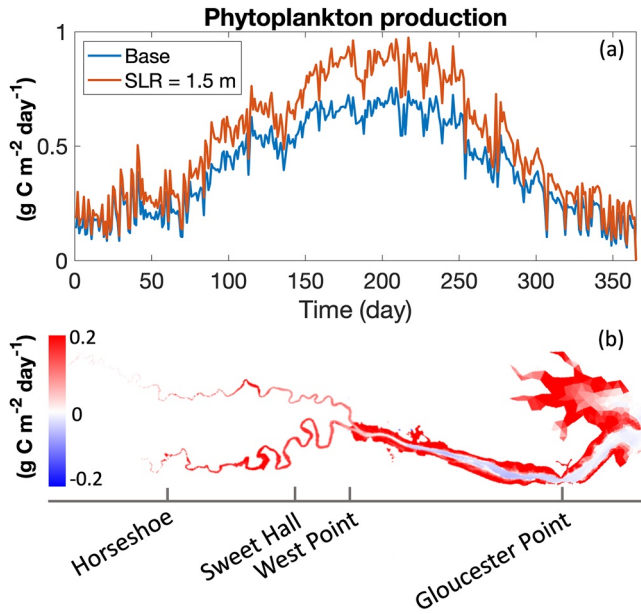


Figure 5. (a) Spatially averaged daily phytoplankton production (PP) in the York River Estuary. (b) Difference of annual-averaged PP between sea-level rise = 1.5 m and Base Scenario (SLR-Base).

oceanic, watershed, and atmospheric forcings except for the changes in the oceanside elevation and the bathymetry of tidal marshes. Other processes, such as river discharge, wind, solar radiation, global warming, and nutrient loadings, are kept the same for SLR scenarios in this study; by doing so, we can focus on the investigation of the impacts only driven by SLR.

2.4. Analysis Methods

2.4.1. Marsh Productivity and Phytoplankton Production

In the model, marsh net productivity is calculated by:

$$MPP = \sum_{m=1,2,3} (Plf_m \cdot (1 - Fam_m) - MTlf_m \cdot BMlf_m) \cdot LF_m - MTst_m \cdot BMst_m \cdot ST_m - BMrt_m \cdot RT_m \quad (1)$$

where $m = 1, 2, 3$ is the index of the three tidal marsh groups (salt marsh, brackish marsh, and freshwater marsh). LF , ST , and RT ($g C m^{-2}$) are biomass of leaf, stem, and root of the vegetation, respectively. Plf (day^{-1}) is the growth function of the leaf. Fam is the fraction for active metabolism during photosynthesis. $BMlf$, $BMst$, and $BMrt$ (day^{-1}) are basal metabolism rates of the leaf, stem, and root, respectively. $MTlf$ and $MTst$ are seasonal mortalities of leaf and stem. Local areal PP is computed by integrating volumetric PP in the water column for each element:

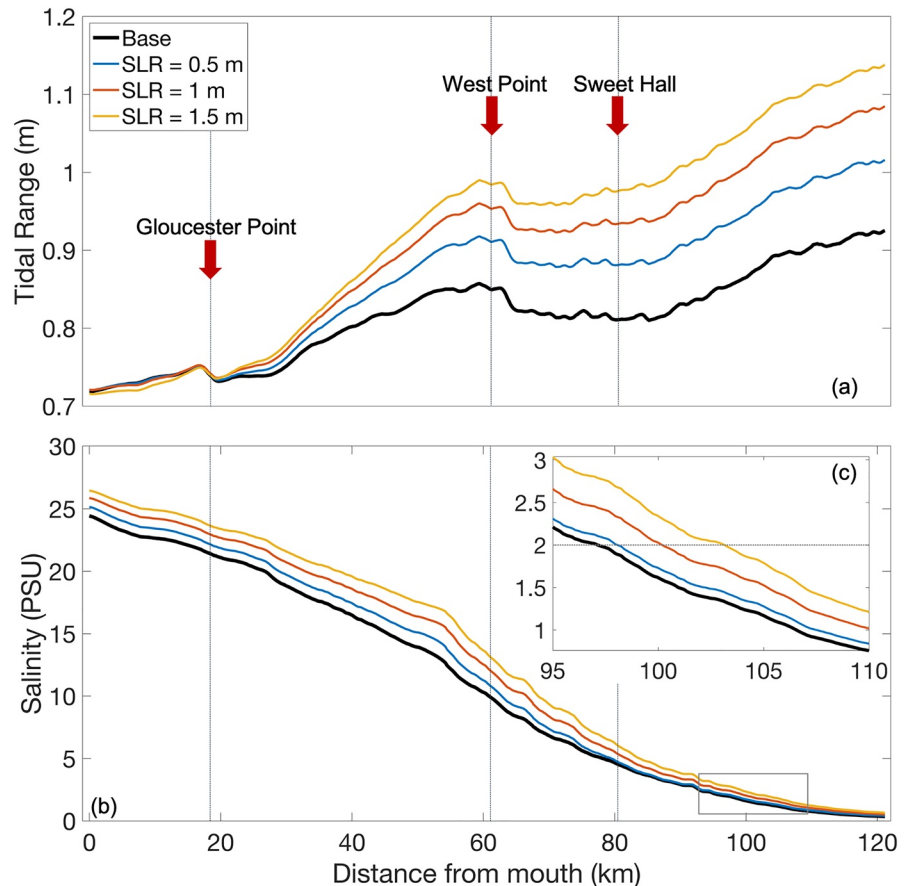


Figure 6. Response of (a) tidal range and (b) bottom salinity to sea-level rise along the channel of Pamunkey and York River as denoted in Figure 1. (c) Zoom in at locations of limitations of saltwater intrusion.

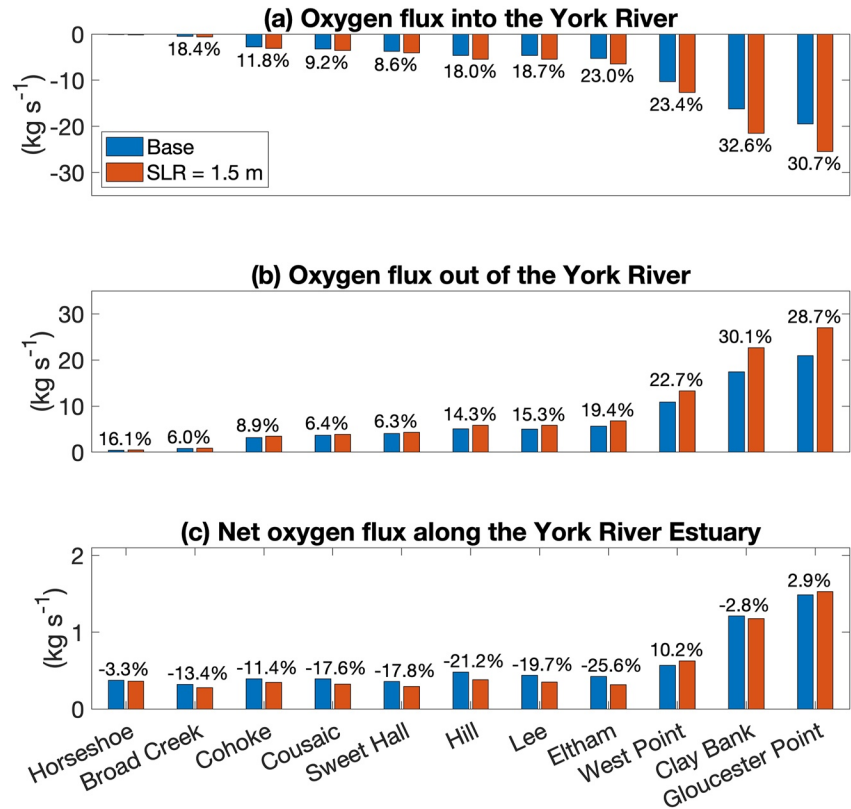


Figure 7. Averages of annual oxygen flux from the upstream of Pamunkey River to the York River mouth in the Base Scenario and sea-level rise (SLR) scenario of 1.5 m. Locations of these cross-sections are denoted in Figures 1c and 1d. Percentage denoted in each panel equals to (SLR-Base)/Base × 100%. In these cross-sections, the influx (negative) corresponds to the direction from the river mouth to the upstream and the outflux (positive) corresponds to the direction from upstream to downstream.

$$GPP = \sum_{i=1}^n (C1_i \cdot G1_i + C2_i \cdot G2_i + C3_i \cdot G3_i) \cdot dep_i \quad (2)$$

where GPP is areal gross primary production of phytoplankton (g C m⁻² day⁻¹), *n* is the number of vertical layers in each element, *i* is the vertical layer index, C1, C2, C3 are carbon-based phytoplankton biomass of three

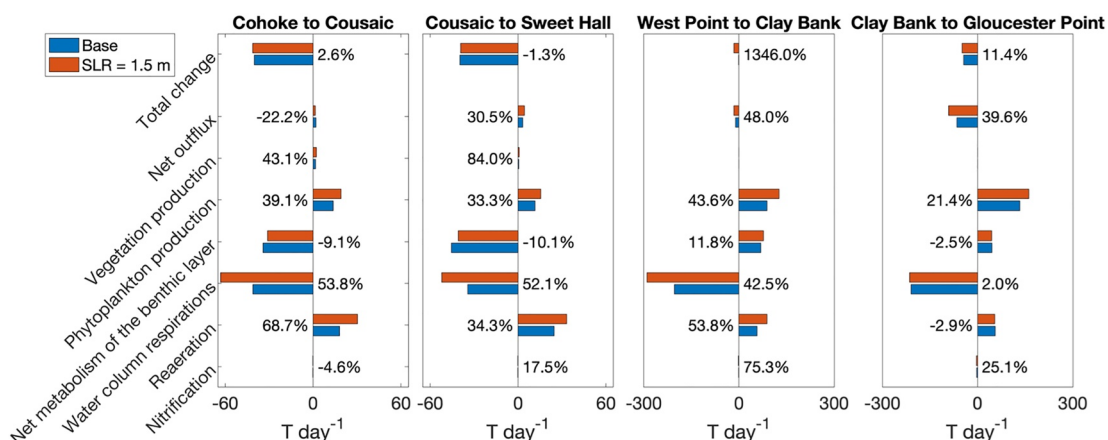


Figure 8. Averaged contribution of each physical or biological process to the dissolved oxygen budget from June to August in the sections where the interfaces are denoted in Figures 1c and 1d. The change percentage (SLR-Base)/Base is labeled.

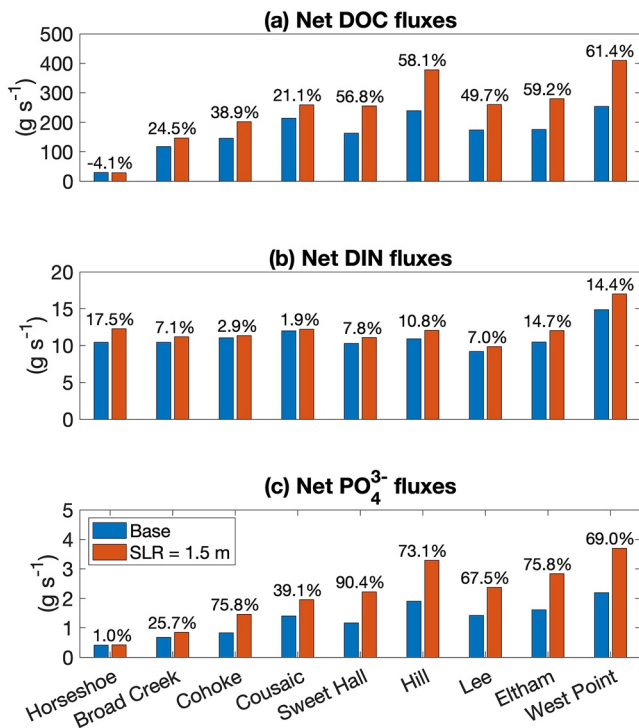


Figure 9. Net fluxes of (a) dissolved organic carbon, (b) dissolved inorganic nitrogen, and (c) total inorganic phosphate from the upstream of Pamunkey River to the downstream in the Base Scenario and sea-level rise (SLR) scenario of 1.5 m. Locations of these cross-sections are denoted in Figure 1d. Percentage denoted in each panel equals to (SLR-Base)/Base × 100%. In these cross-sections, the influx (negative) refers to the direction from the river mouth to the upstream and the outflux (positive) refers to the direction from upstream to downstream.

groups (diatoms, green algae, and cyanobacteria) over each layer respectively (g C m^{-3}), G_1 , G_2 , G_3 are growth rates of the three phytoplankton groups (day^{-1}), and dep is layer thickness (m).

2.4.2. Material Fluxes

Annual-averaged net material fluxes were calculated along the 11 interfaces from the upstream to the downstream (Figures 1b and 1d). Net fluxes of dissolved organic carbon (DOC), DO, and inorganic nutrients were analyzed in the Base Scenario and the SLR scenario. The net flux is the result of outflux (seaward) minus influx (landward), both of which were calculated as the sectionally integrated products of the flow velocity across the interface and the concentrations of the studied material.

$$\text{net flux} = \text{outflux} - \text{influx} = \int_A (u_n \cdot \text{Var}) dA \quad (3)$$

where u_n is the cross-interface velocity (m s^{-1}), Var is the concentration of DOC or other nutrients, A is the vertical area of the interface (m^2). Positive values denote net outflux while negative values denote net influx. Averages of annual and monthly net fluxes were calculated at the selected interfaces.

2.4.3. Oxygen Dynamics

Besides the calculations on oxygen fluxes at each interface denoted in Figures 1b and 1d, each of the major local kinetic processes that affect the oxygen dynamics were calculated in the 10 sections divided by the 11 interfaces. The major local kinetic processes analyzed include the sources of oxygen from vegetation and PP, the sink or source from net metabolism of the benthic layer, the sink to water column respiration, reaeration, and sinks to nitrification. These rates at each section were vertically integrated and then horizontally averaged by the weight of each element area, and the sectionally-averaged values are averaged from June to August. The sum of these local changing terms and the net flux is the total changes of the oxygen budget in this section during the selected period.

3. Response of the Estuarine Biogeochemical Processes to SLR

3.1. Tidal Marshes

Overall, SLR causes a minor decrease in marsh biomass and productivity in most areas of the tidal marshes in the York River Estuary in this modeling study, where marsh habitats are assumed to survive with sufficient vertical accretion (Figures 2c–2e). The decrease in marsh biomass mostly happens in summer and fall (Figure 2e). On the scale of all the marshes in the York River Estuary, the annual decreases of marsh biomass and productivity are on the order of 20 g C m^{-2} and $0.04 \text{ g C m}^{-2} \text{ day}^{-1}$, respectively. In other words, the annual decrease in total marsh biomass is minor (5.18%) compared with the base value (Figure 2e). Besides the minor change in biomass and productivity under SLR, the changes in the amount of local nutrient uptake and release from marsh photosynthesis and metabolism are also small, which is on the order of $3.6 \times 10^{-3} \text{ g N m}^{-2} \text{ day}^{-1}$ and $1.1 \times 10^{-4} \text{ g P m}^{-2} \text{ day}^{-1}$, respectively. Thus, the changes in marsh biomass and productivity have a negligible impact on the material exchanges between the tidal marshes and the channel under SLR.

The comparisons of the Base and SLR Scenarios on the three limiting factors (inundation stress, light limitation, and salinity stress) of marsh leaf growth suggest the predicted decreases in marsh biomass and productivity under SLR are dominated by the increased inundation stress (Figure 3a). These limiting factors are dimensionless, ranging from 0 to 1 (Cai et al., 2023a). The change in the inundation stress is mainly driven by the change in tidal range and plant height. Some observations indicate that the plant height along with the marsh biomass can increase in response to the increased tidal range so that the inundation stress will not limit the growth of the marshes (Morris et al., 2002). For this study, the long-term response of marsh biomass to the change in the tidal range under SLR is not simulated by the model, so the parameters to determine the height based on the above-ground biomass are assumed unchanged. Therefore, the modeled inundation stress

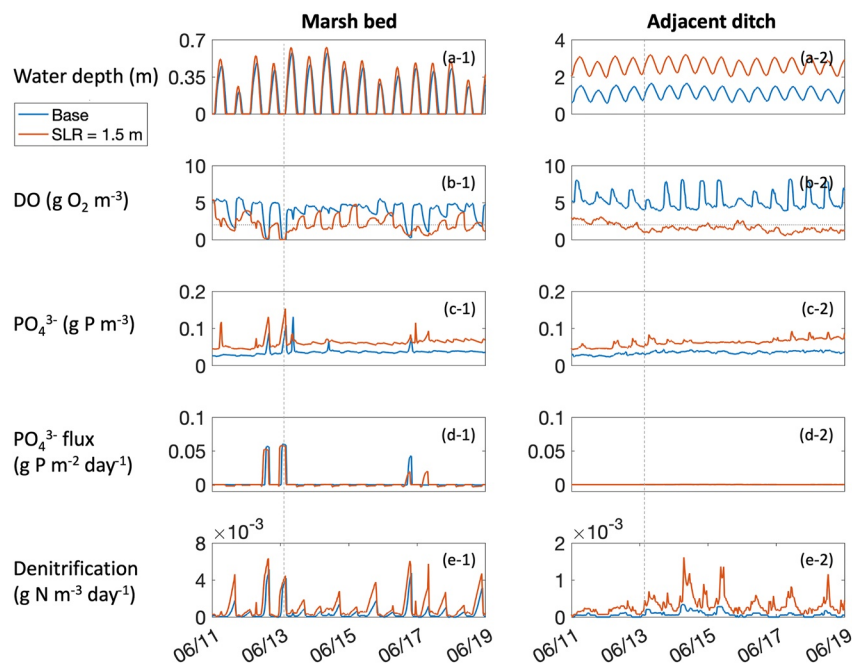


Figure 10. A 9-day window in summer of the simulated water properties (a) local water depth, (b) dissolved oxygen (DO), (c) phosphate, and (d) denitrification rates at two Sweet Hall Marsh stations respectively in the tidal creek and marsh bed (denoted in Figure 1), where only the marsh bed had 1.5 m of vertical accretion under sea-level rise. These two stations are denoted in Figure 1c. The gray dotted horizontal line in (b) denotes a DO concentration of 2 g m^{-3} . Gray dotted vertical lines denote moments of a typical low tide along with low DO, high phosphate, and high denitrification loss.

increases. Given the identical solar radiation in the Base and SLR scenario, the change in light limitation is mainly driven by the change in water column attenuations and self-shading, which is dominated by plant height and biomass. Other conditions, such as the alleviation of light limitation, help to increase salt marsh plant productivity, which results in a minor increase in annual marsh biomass and productivity in certain areas and periods (Figure 3b). The model also suggests there is a shift in marsh species from tidal freshwater marsh to the brackish marsh and brackish marsh to the salt marsh in response to the salinity gradient (not shown in figure), but the total biomass changes little due to the identical parameters of the multiple marsh groups.

3.2. Nitrogen and Phosphorus

The model results show that the changes of inorganic nutrients have different trends upstream and downstream. NH_4^+ and PO_4^{3-} concentrations increase under SLR upstream above West Point where extensive marshes exist, but slightly decrease in the downstream York River (Figures 4c and 4e). Meanwhile, the concentrations of NO_3^- decrease in most areas of the York River Estuary under SLR (Figure 4d). The overall decrease in nutrients in the downstream York River indicates that more nutrients are taken up by phytoplankton to support the increased PP in the York River Estuary as suggested in Figure 5. The increase in NH_4^+ concentration upstream can be up to about 0.007 g N m^{-3} and the decrease in the NO_3^- concentration is less than 0.02 g N m^{-3} (Figures 4c and 4d). An increase of NH_4^+ accompanied by a decrease of NO_3^- is mainly due to changes in PP and nutrient recycling. The decrease in NO_3^- concentration is also attributed to the overall lower DO level and frequent occurrence of temporal hypoxia in the estuary under SLR (Figures 4a, 4d, and 10b). The lower DO level inhibits or slows down the nitrification process, while it favors the denitrification process. Both the increases of NH_4^+ and decrease of NO_3^- contribute to the response of DIN, which mostly decreases in the estuary but slightly increases in the lower part of Pamunkey River. The PO_4^{3-} concentration increases by about 0.07 g P m^{-3} (174.6%) at the open water above Lily Point (Figure 1d). The increase of PO_4^{3-} in the upper estuary is highly related to the overall lower DO and the enhanced sediment fluxes.

3.3. Phytoplankton Production

SLR increases the spatially averaged PP in the entire York River Estuary by 27.9% (Figure 5). In the shallow waters, PP mostly increases by up to $0.6 \text{ g C m}^{-2} \text{ day}^{-1}$ (Figure 5b) and the chlorophyll-a concentration also increases (not shown). The chlorophyll-a concentration in the Pamunkey River channel slightly increases by about $0.5 \text{ }\mu\text{g/L}$ (8.5%), but slightly decreases by $0.6 \text{ }\mu\text{g/L}$ (7.0%) in the York River channel where PP also decreases by $0.05 \text{ g C m}^{-2} \text{ day}^{-1}$ (Figure 5b). The predicted trend of PP in shallow shoals under SLR is the same as that in the Bay shallow waters (Cai et al., 2021), where the increase in shallow water habitat area and light utilization by chlorophyll-a is suggested to be the governing factor leading to the increase in PP under SLR. Since the model accurately represents the shallow water without smoothing the bathymetry, the change of shallow water habitat area is better simulated. However, the nutrient limitation can be observed in the York River main channel (indicated by the lowered nutrient concentrations) also plays a role in slightly decreasing chlorophyll-a concentration in the York River mainstem under SLR (Figures 4e, 4f, and 5b).

3.4. Oxygen and Dissolved Organic Carbon

DO is predicted to significantly decrease upstream adjacent to the extensive marshes while slightly increasing in the York River (Figures 4a and 10b). The decrease of bottom DO is up to about $1.8 \text{ g O}_2 \text{ m}^{-3}$ (21.7%) in the Pamunkey River (Figure 4a). Given the situation that the water is generally mixed in this region (Friedrichs, 2009), the increased DOC caused by greater heterotrophic respiration decreases the bottom DO concentrations in the meanders. The overall lower DO level, accompanied by more low-DO events, prompts more nutrient (i.e., NH_4^+ and PO_4^{3-}) release from the sediment, which in return increases the nutrient availability (Figures 4c and 4e). A detailed analysis of DO dynamics under SLR with consideration of physical transport is presented in the next section.

Under SLR, the DOC concentration shows a clear increase over the upstream of the York River Estuary (Figure 4b). In the Pamunkey River, the increase in DOC concentration is up to 5.3 g C m^{-3} (85.7%) compared with the original concentration in the Base Scenario. A significant fraction of increased DOC in the upper streams is directly related to the increases in chlorophyll-a and PP in the Pamunkey and Mattaponi channels (Figure 5b), and the rest of the DOC increase is affected by the marshes. Despite a slight decrease in marsh biomass and subsequently lower detritus levels, the overall reduction in DO concentration slows down the oxidation of marsh detritus. As a result, a higher amount of DOC accumulates in the bottom of the water column and porewater. These DOC are transported between the marshes and surrounding waters during each tidal cycle and contribute to the total increase in DOC in the system. Downstream West Point, the increase in PP in the shallow shoals plays a significant role in increasing the DOC concentration, though the surface channel shows a slight decrease (Figure 4b).

4. Contributions of the Physical Processes

4.1. Tidal Range and Flooding in the Marshes

Under SLR, the tidal range generally increases toward upstream (Figure 6a). The increased tidal range is consistent with the prediction by the conceptual model in Cai et al. (2022) and model prediction in the James River (Y. Wang & Shen, 2020), which suggests that significant reductions in frictional dissipation play a dominant role. The increase in tidal range is more pronounced toward upstream from the mouth of the York River and gradually becomes “linear” after passing Sweet Hall. The mean increase in tidal range in the York section is about 3.8 cm (4.9%) when SLR is 1.5 m, while it can be about 17.4 cm (20.4%) and 13.4 cm (14.8%) in the Pamunkey and Mattaponi sections, respectively. The increase in the tidal range under SLR is one of the significant factors contributing to the increased outfluxes from the tidal marshes to the open water. The mean depth of the inundated area, including the marsh with vertical accretion, increases by 13.7% in the Pamunkey River under an SLR of 1.5 m (Cai et al., 2022). Duration of the tidal inundations increases significantly over the marshes together with the increased tidal range. For example, in the randomly selected sampling stations in the Sweet Hall Marsh, the inundation period increased by about 0.5 hr in a tidal cycle (Figure 10a-2). The enhanced inundation in tidal marshes promotes the material exchange between the surrounding water and marsh beds. More particulate matters settle down, while dissolved nutrients are released into the flooding water. As a result, despite the overall slightly decreased marsh biomass, tidal marshes contribute to the increased nutrient fluxes from the upstream to the downstream York River.

In this study, the SLR scenario is designed with idealized marsh vertical accretions, but in reality, marsh evolution can be anywhere between fully keeping up with SLR and degrading to tidal flats, depending on the supplies of sediments or the shift in the local marsh community (Mitchell et al., 2017; Reed, 1990, 1995). Predictions from Cai et al. (2022) suggest that the tidal range may increase less than the ideal fully “keep-up” scenario or even decrease if the marsh vertical accretion is smaller than the SLR or if the waterfront marshes degrade into tidal flats in a significant area. If the tidal marsh platform reaches equilibrium at a middle bed elevation, the outflux of material from the tidal marshes will likely have less increase than our current prediction or even show a decrease, and the outflux will also have a smaller or even opposite impact on the estuarine biogeochemical processes than our current predictions due to nonlinear interactions.

4.2. Saltwater Intrusion and Estuarine Circulation

Besides the change in the local tidal range driven by the SLR, the change in other physical processes can also significantly affect the estuarine biogeochemical processes in the York River Estuary, such as the enhanced saltwater intrusion. For example, under an SLR of 1.5 m, the annual average salinity increases from 9.5 to 12.7 PSU at West Point, and from 4.6 to 6.1 PSU at the Sweet Hall Marsh (Figure 6b). The intrusion length is also moved by 5.95 km from the Cohoke Marsh to upstream (2 PSU; Figure 6c). The intrusion length in the York River is in the same order of magnitude as the James River (Rice et al., 2012; Y. Wang & Shen, 2020). The increase in local salinity in these marshes alters the composition of the tidal marsh community in the transition region from the brackish zone to the tidal freshwater zone. For example, the fraction of brackish marshes in the entire simulated marshes increases by 9.84% (cf. Figure 1d). In addition, salinity increase in these regions contributes to depressing the local nitrification while enhancing the bottom release of ammonium and phosphate to the overlying flooding water.

SLR increases the estuarine stratification in the York River Estuary, similar to the predictions for Chesapeake Bay (Cai et al., 2021). As suggested by the calculated oxygen fluxes along the York Estuary in Figures 7a and 7b, the enhanced exchange flow increases both the seaward and landward fluxes of oxygen. However, local changes in DO production and consumption impact the net outfluxes of oxygen from the York River Estuary to the Bay. The net oxygen fluxes show an increasing trend toward the mouth of the York (Gloucester Point) (Figure 7c). This trend persists under SLR, but there is a 2.9% increase in the net oxygen outflux at GP while a reduction of up to 25.6% occurs at interfaces above West Point (Figure 7c). The minor increase in DO outfluxes at GP may be due to an overall increase in productivity including PP in the York River (Figure 5).

5. DO Dynamics in the York River Estuary

Overall, the responses of bottom DO to SLR are predicted to decrease in the channel of York River Estuary in this modeling study (Figure 4a). Multiple processes (e.g., heterotrophic respiration, PP, and estuarine stratification) contribute to this prediction, which needs a synthetic analysis of the underlying mechanisms. The total change and each oxygen-related process in summer have distinct patterns in the upstream sections between one or two marshes (e.g., from the Cohoke to the Cousaic Marsh; Figure 1d) and the downstream York River sections (e.g., from the West Point to the Clay Bank; Figure 1d) (Figure 8). The marsh sections tend to have a larger total change (not necessarily total percentage change) than the York River sections (Figure 8). Overall, the net fluxes via transport are more negligible than the local oxygen dynamics, except for the lower York section (Figure 8). The oxygen source from PP is larger in the York River sections, though the inundated marsh occasionally produces oxygen to the marsh sections (Figure 8). The net metabolism of the benthic layer, which includes the production and consumption of oxygen by benthic algae and the sediment oxygen demand, tends to be a sink of oxygen in the marsh sections but a source to the York River sections (Figure 8). The water column respiration is the largest sink term of oxygen in all these sections, while the average increase in the water column respiration is much larger (about 50%) in the marsh sections than in the York River sections (Figure 8). All those sections take oxygen from the atmosphere, and the marsh sections, which have stronger mixing, take more oxygen, and have larger increases in reaeration under SLR than the York River sections (Figure 8). The oxygen sink to nitrification in the water column is generally negligible (Figure 8). Under SLR, the increase in DOC in the upper streams results in elevated water column respiration that consumes oxygen in the marsh sections, and the decreased DO levels prompt a greater release of DOC release from detritus in the benthic layer and marsh beds (Figures 4a and 8).

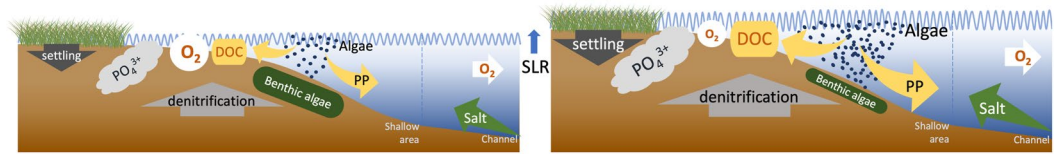


Figure 11. Conceptual diagram of the impacts of sea-level rise on the biogeochemical processes in an estuary with extensive marshes.

6. Material Transport Along the York River Estuary

Under SLR, the net fluxes of DOC increase significantly from the upstream to the downstream locations, which can reach 61.4% in the West Point (Figure 9); and the net fluxes increase by 25.2%, and 11.8% across the Clay Bank, and Gloucester Point, respectively in the downstream York River. The increase of net DOC fluxes is much smaller downstream of the York River than upstream of the Pamunkey River, where extensive marshes and shallow water habitats exist. The changes in net DOC fluxes are the results of changing estuarine circulation, pelagic PP, benthic algae, and marsh contributions. Besides the enhanced circulation, which tends to increase the outfluxes from the upper productive layer. The increase in DOC from pelagic PP contributes significantly to the whole budget and the net fluxes. On the other hand, the lower bottom DO (Figure 10b) along with deeper water depth (Figure 10a) and more consumption from the increased DOC from pelagic and benthic algae, slows down the oxidation of detritus of tidal marshes, which further released more DOC. The expansion of tidal flooding area and prolonged duration under SLR enhances the porewater exchange of the solute materials between the marsh and the open water. Although more particulate matter becomes trapped within the marsh, a greater amount of DOC is released and transported to the adjacent channel. In conclusion, the significant increase in net DOC fluxes above West Point is primarily caused by the presence of marsh, and this also explains the increase in water column respiration at the upper stream sections (Figure 8). The 11.8% net increase in net DOC fluxes to the Chesapeake Bay tends to contribute to the predicted exacerbation of Bay hypoxia (Cai et al., 2021) by augmenting respiration processes.

Both DIN and PO_4^{3-} fluxes increase, but with different magnitude. For example, DIN and PO_4^{3-} fluxes increase by 14.4% and 64.0%, respectively at West Point. This is mainly due to the change in nutrient recycling and transformation. NH_4^+ is the major driver of increased DIN flux along the Pamunkey River since NO_3^- mostly decreases (Figures 4c, 4d, and 4f). The increase of net PO_4^{3-} fluxes from upstream to downstream is larger than the DIN and particularly higher in the region adjacent to large tidal marshes (Figure 9c). Both the lower DO and increasing salinity depress the nitrification process, which in turn prompts the NH_4^+ . The lower DO is also favorable to denitrification, which releases nitrogen gas and lowers the increase of DIN fluxes compared with the phosphate (Figures 9 and 10d). The overall lower DO promotes more phosphate release from the sediment. Each low-DO event at low tide generates a pulse of phosphate and the dissolved nutrients are exported in phase with tidal fluctuation (Figure 10c).

7. Summary and Conceptual Diagram of the Impacts of SLR on the York River Estuary

We utilized a 3D UG model (SCHISM-ICM-Marsh) to investigate the responses of the tidal marshes and the estuarine biogeochemical processes to SLR in the York River Estuary. The SLR scenarios are conducted with the assumption that the tidal marshes can keep up with the SLR. SLR affects the estuary through multiple biogeochemical processes interacting with each other directly or indirectly (Figure 11). Although the increased tidal range under SLR slightly depresses the marsh biomass and productivity by increasing the inundation stress, the prolonged inundation over marsh beds enhances the material exchange. The material exchange between the tidal marshes and the adjacent channels interacts with the phytoplankton, nutrient, and oxygen dynamics in the estuary. Pelagic PP increases under SLR due to increased shallow water habitat area and enhanced utilization of light supply. Therefore, larger PP leads to larger DOC and thus water column respiration. Bottom DO is generally at a lower level in the upstream channel and tidal marsh beds under SLR, which further increases the DOC release from the benthic algae and marsh detritus by slowing down the local oxidation during the increased inundation period. Prolonged low-DO events increase the phosphate release from the sediment. The decrease in DO level and increase in saltwater intrusion slow down the nitrification, so the sediment ammonium release increases. In addition, lower DO levels prompt denitrification rates, which removes part of the nitrogen out of the estuary.

Overall, the impacts on DIN are relatively minor compared with the others. On the other hand, bottom DO in the lower York River tends to slightly increase because of the increased pelagic PP and gravitational circulation.

For the sake of simplicity, the current study only considers the impact of SLR and neglects other possible impacts such as the change in land use, the adaptation of marsh plants to the changing environment, or the temperature change. Also, this study only focuses on the ideal case that the tidal marshes keep up with the SLR, without explicitly investigating the response of the estuary if there are geomorphological changes on the shoreline or the tidal marsh habitats. Overall, this modeling system tends to encompass the dominant hydrodynamic and biogeochemical processes. For example, as reported by Wilson et al. (2023), the nutrient fluxes via groundwater discharge are much lower than the fluvial inputs. This study neglects the groundwater coupling but is dynamically linked to the watershed loadings. In addition, we did not consider the change in marsh physiology under SLR. The sensitivity tests conducted by Cai et al. (2023a) indicate that variations in marsh physiology, including growth rate, metabolism rate, and optimal growth temperature, have minimal effects on estuarine biogeochemical processes. Therefore, the neglected change in marsh physiology should not undermine the conclusions. On the other hand, the change in land use and temperature are equally extensive in scope compared to SLR resulting from climate change. Our intention is to utilize a modeling approach in this study to isolate the processes of SLR for the research question: how do tidal marshes and estuarine biogeochemical processes respond to SLR? Still, the results shown in this paper serve to elucidate potential complex nonlinear processes that may occur in tidal marshes under future climate change.

Data Availability Statement

The SCHISM model code and post-processing code are available at Cai (2023). The setup and parameter details can be found at Cai et al. (2023a, 2023b). Metadata and data that are derived from raw model outputs and used for analysis are available in the Github repository at Cai et al. (2023c).

Acknowledgments

This research was financially supported by the Virginia Commonwealth Research Fellowship and supported in part by an appointment to the Research Participation Program at the Chesapeake Bay Program Office, U.S. Environmental Protection Agency, Region 3, administered by the Oak Ridge Institute for Science and Education through an interagency agreement between the U.S. Department of Energy and the U.S. Environmental Protection Agency. We received tremendous guidance and supports from Drs. Carl Cerco, Carl Hershner, Mark Brush, and Marjy Friedrichs in this study. Simulations presented in this paper were conducted using Sciclone at William & Mary, which was provided with assistance from the National Science Foundation, the Virginia Port Authority, Virginia's Commonwealth Technology Research Fund, and the Office of Naval Research.

References

- Axelrad, D. M., Moore, K. A., & Bender, M. E. (1976). Nitrogen phosphorus and carbox flux in Chesapeake Bay marshes.
- Bates, B., Kundzewicz, Z., & Wu, S. (2008). Climate change and water. In *Intergovernmental panel on climate change secretariat*.
- Boon, J. D. (2012). Evidence of sea level acceleration at US and Canadian tide stations, Atlantic Coast, North America. *Journal of Coastal Research*, 28(6), 1437–1445. <https://doi.org/10.2112/jcoastres-d-12-00102.1>
- Bridgman, S. D., Megonigal, J. P., Keller, J. K., Bliss, N. B., & Trettin, C. (2006). The carbon balance of North American wetlands. *Wetlands*, 26(4), 889–916. [https://doi.org/10.1672/0277-5212\(2006\)26\[889:tcbona\]2.0.co;2](https://doi.org/10.1672/0277-5212(2006)26[889:tcbona]2.0.co;2)
- Brooks, T. J. (1983). Pamunkey River slack water data report: Temperature, salinity, dissolved oxygen, 1970–1980.
- Cai, X. (2023). schism/icm_Balg [Software]. Zenodo. <https://doi.org/10.5281/zenodo.8067380>
- Cai, X., Qin, Q., Shen, J., & Zhang, Y. J. (2022). Bifurcate responses of tidal range to sea-level rise in estuaries with marsh evolution. *Limnology and Oceanography Letters*, 7(3), 210–217. <https://doi.org/10.1002/lol2.10256>
- Cai, X., Shen, J., Zhang, Y. J., Qin, Q., & Linker, L. (2023a). The roles of tidal marshes in the estuarine biochemical processes: A numerical modeling study. *Journal of Geophysical Research: Biogeosciences*, 128(2), e2022JG007066. <https://doi.org/10.1029/2022jg007066>
- Cai, X., Shen, J., Zhang, Y. J., Qin, Q., & Linker, L. (2023b). Sea-level rise impacts on tidal marshes and estuarine biogeochemical processes [Dataset]. Virginia Institute of Marine Science. <https://doi.org/10.25773/3g1y-t092>
- Cai, X., Shen, J., Zhang, Y. J., Qin, Q., & Linker, L. (2023c). Sea-level rise impacts on tidal marshes and estuarine biogeochemical processes [Dataset]. Zenodo. <https://doi.org/10.5281/zenodo.7631491>
- Cai, X., Shen, J., Zhang, Y. J., Qin, Q., Wang, Z., & Wang, H. (2021). Impacts of sea-level rise on hypoxia and phytoplankton production in Chesapeake Bay: Model prediction and assessment. *JAWRA Journal of the American Water Resources Association*, 58(6), 922–939. <https://doi.org/10.1111/1752-1688.12921>
- Cai, X., Zhang, Y. J., Shen, J., Wang, H., Wang, Z., Qin, Q., & Ye, F. (2020). A numerical study of hypoxia in Chesapeake Bay using an unstructured grid model: Validation and sensitivity to bathymetry representation. *JAWRA Journal of the American Water Resources Association*, 58(6), 898–921. <https://doi.org/10.1111/1752-1688.12887>
- Cerco, C. F., & Cole, T. M. (1994). *CE-QUAL-ICM: A three-dimensional eutrophication model, version 1.0. User's guide*. US Army Corps of Engineers Waterways Experiments Station.
- Cerco, C. F., & Seitzinger, S. P. (1997). Measured and modeled effects of benthic algae on eutrophication in Indian River-Rehoboth Bay, Delaware. *Estuaries*, 20(1), 231–248. <https://doi.org/10.2307/1352733>
- Cerco, C. F., & Tian, R. (2022). Impact of wetlands loss and migration, induced by climate change, on Chesapeake Bay DO standards. *JAWRA Journal of the American Water Resources Association*, 58(6), 958–970. <https://doi.org/10.1111/1752-1688.12919>
- Chambers, R. M. (1992). A fluctuating water-level chamber for biogeochemical experiments in tidal marshes. *Estuaries*, 15(1), 53–58. <https://doi.org/10.2307/1352709>
- Chassignet, E. P., Hurlburt, H. E., Smedstad, O. M., Halliwell, G. R., Hogan, P. J., Wallcraft, A. J., et al. (2007). The HYCOM (hybrid coordinate ocean model) data assimilative system. *Journal of Marine Systems*, 65(1–4), 60–83. <https://doi.org/10.1016/j.jmarsys.2005.09.016>
- Chmura, G. L., Anisfeld, S. C., Cahoon, D. R., & Lynch, J. C. (2003). Global carbon sequestration in tidal, saline wetland soils. *Global Biogeochemical Cycles*, 17(4), 1111–1. <https://doi.org/10.1029/2002gb001917>
- Craft, C., Clough, J., Ehman, J., Joye, S., Park, R., Pennings, S., et al. (2009). Forecasting the effects of accelerated sea-level rise on tidal marsh ecosystem services. *Frontiers in Ecology and the Environment*, 7(2), 73–78. <https://doi.org/10.1890/070219>

- Cronin, W. B. (1971). Volumetric, areal, and tidal statistics of the Chesapeake Bay estuary and its tributaries.
- Dauer, D. M., Marshall, H. G., Donat, J. R., Lane, M. F., Doughten, S. C., & Hoffman, F. A. (2007). An update of current status and long-term trends in water quality and living resources in the Virginia tributaries from 1985 to 2005.
- Friedrichs, C. T. (2009). York River physical oceanography and sediment transport. *Journal of Coastal Research*, 10057(10057), 17–22. <https://doi.org/10.2112/1551-5036-57.sp1.17>
- Hong, B., Liu, Z., Shen, J., Wu, H., Gong, W., Xu, H., & Wang, D. (2020). Potential physical impacts of sea-level rise on the Pearl River Estuary, China. *Journal of Marine Systems*, 201, 103245. <https://doi.org/10.1016/j.jmarsys.2019.103245>
- Irby, I. D., Friedrichs, M. A., Da, F., & Hinson, K. E. (2018). The competing impacts of climate change and nutrient reductions on dissolved oxygen in Chesapeake Bay. *Biogeosciences*, 15(9), 2649–2668. <https://doi.org/10.5194/bg-15-2649-2018>
- Jordan, T. E., Cornwell, J. C., Boynton, W. R., & Anderson, J. T. (2008). Changes in phosphorus biogeochemistry along an estuarine salinity gradient: The iron conveyor belt. *Limnology & Oceanography*, 53(1), 172–184. <https://doi.org/10.4319/lo.2008.53.1.0172>
- Jordan, T. E., Correll, D. L., & Whigham, D. F. (1983). Nutrient flux in the Rhode river: Tidal exchange of nutrients by brackish marshes. *Estuarine, Coastal and Shelf Science*, 17(6), 651–667. [https://doi.org/10.1016/0272-7714\(83\)90032-x](https://doi.org/10.1016/0272-7714(83)90032-x)
- Kuo, A. Y., & Neilson, B. J. (1987). Hypoxia and salinity in Virginia estuaries. *Estuaries*, 10(4), 277–283. <https://doi.org/10.2307/1351884>
- Mesinger, F., DiMego, G., Kalnay, E., Mitchell, K., Shafran, P. C., Ebisuzaki, W., et al. (2006). North American regional reanalysis. *Bulletin of the American Meteorological Society*, 87(3), 343–360. <https://doi.org/10.1175/bams-87-3-343>
- Mitchell, M., Herman, J., Bilkovic, D. M., & Hershner, C. (2017). Marsh persistence under sea-level rise is controlled by multiple, geologically variable stressors. *Ecosystem Health and Sustainability*, 3(10), 1379888. <https://doi.org/10.1080/20964129.2017.1396009>
- Molino, G. D., Carr, J. A., Ganju, N. K., & Kirwan, M. L. (2022). Variability in marsh migration potential determined by topographic rather than anthropogenic constraints in the Chesapeake Bay region. *Limnology and Oceanography Letters*, 7(4), 321–331. <https://doi.org/10.1002/lo2.10262>
- Morris, J. T., Sundareshwar, P. V., Nietch, C. T., Kjerfve, B., & Cahoon, D. R. (2002). Responses of coastal wetlands to rising sea level. *Ecology*, 83(10), 2869–2877. [https://doi.org/10.1890/0012-9658\(2002\)083\[2869:ROCWTR\]2.0.CO;2](https://doi.org/10.1890/0012-9658(2002)083[2869:ROCWTR]2.0.CO;2)
- Neubauer, S. C., & Craft, C. B. (2009). *Global change and tidal freshwater wetlands: Scenarios and impacts* (pp. 253–266). Tidal freshwater wetlands.
- Nichols, M. M., Kim, S. C., & Brouwer-Riel, C. (1991). *Sediment characterization of the Chesapeake Bay and its tributaries, Virginian Province*. School of Marine Science, Virginia Institute of Marine Science, College of William and Mary.
- Reay, W. G. (2009). Water quality within the York River estuary. *Journal of Coastal Research*, 10057(10057), 23–39. <https://doi.org/10.2112/1551-5036-57.sp1.23>
- Reed, D. J. (1990). The impact of sea-level rise on coastal salt marshes. *Progress in Physical Geography*, 14(4), 465–481. <https://doi.org/10.1177/030913339001400403>
- Reed, D. J. (1995). The response of coastal marshes to sea-level rise: Survival or submergence? *Earth Surface Processes and Landforms*, 20(1), 39–48. <https://doi.org/10.1002/esp.3290200105>
- Rice, K. C., Hong, B., & Shen, J. (2012). Assessment of salinity intrusion in the James and Chickahominy rivers as a result of simulated sea-level rise in Chesapeake Bay, East Coast, USA. *Journal of Environmental Management*, 111, 61–69. <https://doi.org/10.1016/j.jenvman.2012.06.036>
- Rysgaard, S., Thastum, P., Dalsgaard, T., Christensen, P. B., & Sloth, N. P. (1999). Effects of salinity on NH_4^+ adsorption capacity, nitrification, and denitrification in Danish estuarine sediments. *Estuaries*, 22(1), 21–30. <https://doi.org/10.2307/1352923>
- Santoro, A. E. (2010). Microbial nitrogen cycling at the saltwater–freshwater interface. *Hydrogeology Journal*, 18(1), 187–202. <https://doi.org/10.1007/s10040-009-0526-z>
- Shen, J., & Haas, L. (2004). Calculating age and residence time in the tidal York River using three-dimensional model experiments. *Estuarine, Coastal and Shelf Science*, 61(3), 449–461. <https://doi.org/10.1016/j.eess.2004.06.010>
- Shenk, G. W., & Linker, L. C. (2013). Development and application of the 2010 Chesapeake Bay watershed total maximum daily load model. *JAWRA Journal of the American Water Resources Association*, 49(5), 1042–1056. <https://doi.org/10.1111/jawr.12109>
- Sin, Y., Wetzel, R., Lee, B. G., & Kang, Y. (2006). Integrative ecosystem analyses of phytoplankton dynamics in the York River estuary (USA). *Hydrobiologia*, 571(1), 93–108. <https://doi.org/10.1007/s10750-006-0232-y>
- Sin, Y., Wetzel, R. L., & Anderson, I. C. (1999). Spatial and temporal characteristics of nutrient and phytoplankton dynamics in the York River estuary, Virginia: Analyses of long-term data. *Estuaries*, 22(2), 260–275. <https://doi.org/10.2307/1352982>
- Sprague, L. A. (2000). *Factors affecting nutrient trends in major rivers of the Chesapeake Bay watershed (No. 4218)*. US Department of the Interior, US Geological Survey.
- St-Laurent, P., Friedrichs, M. A., Li, M., & Ni, W. (2019). Impacts of sea level rise on hypoxia in the Chesapeake Bay: A model intercomparison.
- Sutter, L. A. (2014). *Effects of saltwater intrusion on vegetation dynamics and nutrient pools in low-salinity tidal marshes*. The College of William and Mary.
- Wang, P., Linker, L., Wang, H., Bhatt, G., Yactayo, G., Hinson, K., & Tian, R. (2017). Assessing water quality of the Chesapeake Bay by the impact of sea level rise and warming. In *IOP conference series: Earth and environmental science* (Vol. 82, p. 012001). IOP Publishing.
- Wang, Y., & Shen, J. (2020). A modeling study on the influence of sea-level rise and channel deepening on estuarine circulation and dissolved oxygen levels in the tidal James River, Virginia, USA. *Journal of Marine Science and Engineering*, 8(11), 950. <https://doi.org/10.3390/jmse8110950>
- Wilson, S. J., Anderson, I. C., Song, B., & Tobias, C. R. (2023). Temporal and spatial variations in subterranean estuary geochemical gradients and nutrient cycling rates: Impacts on groundwater nutrient export to estuaries. *Journal of Geophysical Research: Biogeosciences*, 128(6), e2022JG007132. <https://doi.org/10.1029/2022jg007132>
- Zhang, Y. J., Gerdts, N., Ateljevich, E., & Nam, K. (2020). Simulating vegetation effects on flows in 3D using an unstructured grid model: Model development and validation. *Ocean Dynamics*, 70(2), 213–230. <https://doi.org/10.1007/s10236-019-01333-8>
- Zhang, Y. J., Ye, F., Stanev, E. V., & Grashorn, S. (2016). Seamless cross-scale modeling with SCHISM. *Ocean Modelling*, 102, 64–81. <https://doi.org/10.1016/j.ocemod.2016.05.002>